Effects of Al(MnFe)Si dispersoids with different sizes and number densities on microstructure and ambient/elevated-temperature mechanical properties of extruded Al-Mg-Si AA6082 alloys with varying Mn content

Jovid Rakhmonov [a*], Kun Liu [a], Paul Rometsch [b], Nick Parson [b], X.-Grant Chen [a]**

[a] Department of Applied Science, University of Quebec in Chicoutimi, Saguenay, Quebec, QC, G7H 2B1, Canada
[b] Arvida Research and Development Center, Rio Tinto Aluminum, Saguenay, Quebec, G7S 4K8, Canada

* Corresponding author: J. Rakhmonov (jovid.rakhmonov1@uqac.com)
** Corresponding author: K. Liu (kun.liu@uqac.com)

Abstract

The effects of Al(MnFe)Si dispersoids, with different sizes and number densities, on the evolution of microstructure and ambient/elevated-temperature mechanical properties of extruded AA6082 alloys, with varying Mnntent, under T5 conditions, were investigated. Compared to the low density of coarse dispersoids formed during conventional homogenization, the high density of fine dispersoids formed during a new low-temperature homogenization was more effective in increasing the material's resistance to plastic deformation during extrusion, resulting in the dissolution of more constituent Mg_2Si particles into the α-Al matrix. A large amount of β'', some β' precipitates and fine dispersoids co-existed in the α-Al matrix of 0.5% Mn containing alloy, which afforded this alloy a substantial increase in ambient-temperature yield strength of 65-75 MPa under T5 conditions compared to the base alloy without dispersoids. A further increase in the Mn content decreased the number density of the β'' precipitates, resulting in a decline in the mechanical properties. Upon thermal exposure at 300 °C for 100 h, β''/β' fully transformed into an undesirable equilibrium β phase and lost their strengthening effect, while fine and dense dispersoids became the dominant strengthener, leading to a 55-70% increase in the elevated-temperature yield strength relative to the alloys either without dispersoids or with coarse dispersoids. Dispersoid strengthening was more pronounced at 0.7% Mn addition as further increasing the Mn content mainly contributed to the fraction of insoluble Mn-containing intermetallics.

Keywords: Al-Mg-Si AA6082 alloy; Extrusion; Al(MnFe)Si dispersoids; Microstructure; Mechanical properties.

1. Introduction

Owing to their high strength/weight ratio, good formability, and excellent corrosion resistance, Al-Mg-Si AA6082 alloys are widely used as structural materials in the transport and building industries [1]. A combination of (a) the nanoscale Mg_2Si precursor precipitates that form during artificial aging and (b) the fibrous grain structure obtained during hot deformation due to the formation of dispersoids during homogenization, provides a relatively high strength to the AA6082 alloys of the Al-Mg-Si 6xxx family [2]. AA6082 alloys are suitable for highly stressed applications with service temperatures generally not exceeding 150 °C. However, at higher temperatures the strength of AA6082 alloys significantly decreases owing to the rapid coarsening of β''/β'-MgSi precipitates [3].

In common industrial practice, homogenization prior to extrusion is conducted at a relatively high temperature, typically at 550 °C for AA6082 alloys, which results in the formation of coarse Al(FeMn)Si dispersoids (~200 nm in diameter) in the α-Al matrix [4, 5]. These dispersoids provide the alloy with limited dispersion strengthening through the Orowan bypass mechanism [6]. Attempts to enhance the dispersion strengthening effect in various Al-based alloys have been the subject of multiple studies [7-11], as these dispersoids are (1) resistant to coarsening at temperatures up to 400 °C and (2) comparably less expensive than the nano-sized trialuminides alloyed with Sc, Zr, or Er. The introduction of solid-state precipitation of fine and dense dispersoids improves the high-temperature mechanical properties of aluminum alloys [10-14]. Recent studies have focused on enhancing the characteristics of dispersoids by optimizing the heat treatment [15, 16], enriching the dispersoids with slow-diffusing transition elements [8, 11, 17], and promoting the nucleation of dispersoids [3, 13].

Recently, Li et al. [18] investigated the precipitation behavior of dispersoids in AA6082 alloys and reported that Al(FeMn)Si dispersoids with an optimum size and distribution can be obtained by low-temperature homogenization at 400 °C. Moreover, such dispersoids showed a limited coarsening tendency during heat treatment at 400 °C upon prolonged soaking times. Qian et al. [19] studied the role of Al(FeMn)Si dispersoids formed during the homogenization of AA6082 alloys on the softening processes, such as recovery and recrystallization, during hot compressive deformation and subsequent heat treatment. The dispersoids can effectively retard recrystallization during both hot deformation and post-deformation annealing.

AA6082 alloys are predominantly processed through extrusion operations to manufacture aluminum structural components. The peak temperature during extrusion can typically reach as high as 550 °C, at which coarsening of the dispersoids becomes active. The response of AA6082 alloys with fine and dense Al(FeMn)Si dispersoids to extrusion processing has not previously been evaluated. Moreover, the effects of Mn content and related dispersoids on the microstructure evolution during extrusion, along with the precipitation behavior of β''/β'-MgSi precipitates during the aging treatment, are unknown. The possibility of incorporating fine and dense dispersoids in addition to β''/β' precipitates into the α-Al matrix of AA6082 alloys might enhance its mechanical response to thermal exposure; this is a novel and cost-effective approach to enhance the high-temperature mechanical properties of aluminum structures during service. This study aimed to investigate the effects of varying Mn content and related dispersoids on the microstructural evolution during extrusion and aging and on the ambient/elevated-temperature mechanical properties of AA6082 alloys.

2. Experimental procedures

2.1 Materials and pre-extrusion heat treatment

The DC cast billets (100 mm in diameter) from four variants of AA6082 type alloys were provided by the Arvida Research and Development Centre of Rio Tinto Aluminium, Quebec. The chemical compositions analyzed by optical emission spectroscopy are shown in

Table 1. The average secondary dendrite arm spacing (SDAS) at the center and mid-radius of all cast billets was measured to be ~17 μm, suggesting a good reproducibility of the temperature profile during DC casting.

Table 1. Chemical compositions of the DC cast AA6082 alloys (wt.%)

Alloys	Mg	Si	**Mn**	Fe	Ti
0 Mn	0.83	1.01	**0.00**	0.22	0.016
0.5% Mn	0.84	1.02	**0.50**	0.23	0.016
0.7% Mn	0.84	1.02	**0.72**	0.23	0.015
1% Mn	0.81	1.02	**1.00**	0.24	0.015

Based on the results of the initial trials, the cast billets were heat-treated at 400 °C for 5 h to induce the formation of a large number density of Al(FeMn)Si dispersoids in the α-Al matrix. The four alloy variants were heat-treated at 400 °C for 5 h, and are hereafter referred to as 0Mn, 0.5Mn(L), 0.7Mn(L) and 1Mn(L) alloys, respectively (see Table 2). Some billets containing 0.5% Mn were also subjected to a common industrial homogenization at 550 ºC for 5 h (hereafter referred to as 0.5Mn(H) alloy) to compare the strengthening effect of dispersoids with different sizes and number densities. The heating rate for both heat treatments was set at 100 °C/h.

Table 2. The heat treatments applied for various alloys prior to extrusion

Alloys	Heat treatments	Alloy codes
0 Mn	400 °C / 5 h	**0Mn**
0.5% Mn		**0.5Mn(L)**
0.7% Mn		**0.7Mn(L)**
1% Mn		**1Mn(L)**
0.5% Mn	550 °C / 5 h	**0.5Mn(H)**

2.2 Extrusion and post-extrusion heat treatment

The heat-treated billets were extruded by sequential pre-heating, extrusion, and quenching steps. The billets were pre-heated to 500 °C via induction heating for ~5 min and quickly transferred to the press. Billets were extruded at a ram speed of 10 mm/s to produce round bars with a diameter of 17.8 mm. The temperature of the extruding rods at the exit of the press was manually measured using a K-type thermocouple. To retain the microstructure upon extrusion, the rods were quenched in a water bath. Samples of extruded rods were aged at 180 °C for 5 h for the T5 temper. In addition, some of the T5 treated samples were further exposed at 300 °C for 100 h to determine the elevated-temperature strength [9, 18].

2.3 Material characterization

The microstructure of the alloys was characterized using optical microscopy (OM), scanning electron microscopy (SEM) equipped with electron backscatter diffraction (EBSD) and transmission electron microscopy (TEM). Sample grinding and polishing were performed according to the standard metallographic procedure. Final polishing step was processed with 0.05 µm colloidal silica suspension. Samples of as-cast billets for metallographic investigations were sectioned at the mid-radius. To characterize the microstructure of the extruded rods, samples were sectioned so that the viewing plane was maintained parallel to the extrusion direction and passed through the center of the rod. The EBSD scans of the as-extruded alloys possessing un-recrystallized and recrystallized grain structures were performed at step sizes of 0.5 and 5 µm, respectively. The EBSD runs for each condition were assured to have an indexing ratio of at least 85%. The original EBSD datasets were post-processed using HKL Channel 5 software and noise reduction was conducted to remove the non-indexed points. The TEM thin foils were prepared using the following steps: (i) punching a 3 mm diameter specimen, (ii) thinning of the disk-shaped specimen to ~ 50 µm via grinding and polishing and (iii) electro-chemical polishing of the specimen with a twinjet electropolisher at 20 V DC using a solution of 67% methanol and 33% HNO_3 at ~ 20 - 30 °C. The observations of the precipitates and dispersoids in the α-Al matrix were performed using a transmission electron microscope (TEM, JEOL JEM-2100) near the [001] zone axis of the g200 beam condition (operated at 200 kV). The Kossel-Möllenstedt (K-M) fringes in the convergent beam electron diffraction (CBED) pattern, obtained under two-beam condition, were used to measure the TEM foil thickness [20]. The volume fraction of Al(FeMn)Si dispersoids, f_d, was estimated using the following equation [21]:

$$f_d = A_d \frac{\bar{K}\bar{D}}{\bar{K}\bar{D}+t}(1 - A_{DFZ}) \qquad (1)$$

where, $\bar{D}$ is the dispersoid's equivalent diameter calculated according to Ref. [21]; t is the TEM foil thickness, A_d is the percentage area of dispersoids from the TEM images, A_{DFZ} is the percentage area of dispersoid free zones from the OM images; $\bar{K}$ is the average shape factor for dispersoids and the value of 0.45 is accepted in this study. The number density of Al(FeMn)Si dispersoids is estimated by [3]:

$$N_v = \frac{N}{A(\bar{D}+t)} \qquad (2)$$

where, N_v represents the number of dispersoids within the image and A is the area of the image. The number density of the β'' precipitates was derived from [22]:

$$N_v = \frac{3N_t}{A(t+l)} \qquad (3)$$

where, N_t is the number of β'' needles being oriented along the beam direction; l is the average length of the β'' needles, and t is the TEM foil thickness. At least six TEM micrographs captured from different regions of α-Al matrix were used to quantify the precipitates and dispersoids.

The electrical conductivity (EC) of the as-extruded alloys was tested using a Sigmascope SMP10 unit at a frequency of 60 kHz to evaluate the extent of the dissolution of constituent particles during extrusion. The Vickers microhardness tests were conducted under a load of 100 g and dwell time of 20 s. The T5 mechanical properties were characterized by performing a compressive yield strength (YS) test at room temperature. To investigate the elevated-temperature strengths of AA6082-T5 alloys, compressive yield strength tests were conducted at both 20 and 300 °C on the samples after long-term thermal exposure (300 °C/100 h). All compressive yield strength tests were carried out using the Gleeble 3800 thermo-mechanical simulator unit on the samples with a 15 mm length and 10 mm diameter. The strain rate during the test was set at 10^{-3} s^{-1} to reach a total strain of 0.2. For the tests at 300 °C, the samples were preheated to test temperature at a rate of 2 °C/sec and held for 3 min prior to compression loading. Specimen temperature during preheating, holding and compression stages was ensured constant (300 ± 0.2 ºC) using the spot-welded thermocouples on the surface connected to the Gleeble system. Tensile tests were conducted on round-shaped samples at room temperature for the T5 treated alloys using an Instron machine. To obtain reproducible results, at least three samples per condition were tested in the tensile and compression tests.

3. Results and Discussion

3.1 The formation of Al(FeMn)Si dispersoids and their effects on microstructure evolution during extrusion

Fig. 1a shows the Al(FeMn)Si dispersoids in the α-Al matrix of the 0.5Mn(H) alloy before extrusion, which was subjected to an industrial homogenization process at 550 °C for 5 h. Consistent with the literature [21], the dispersoids are mainly platelet-shaped and have an average equivalent diameter ($\overline{D}$) of 156 nm (Table 3). Contrarily, the microstructures of the 0.5Mn(L) and 1Mn(L) alloys before extrusion, which were heat-treated at 400 °C for 5 h, featured much finer ($\overline{D}$ ~ 25 nm) and denser Al(FeMn)Si dispersoids (see Fig. 1b and c and Table 3). The dispersoids in these alloys appear predominantly as platelets (dashed arrows) or cuboids (solid arrows). The evolution of Al(FeMn)Si dispersoids with platelet- and cuboidal-shaped morphologies in aluminum alloys was reported in a recent study by De Luca et al. [23]. The TEM image of the 0.7Mn(L) alloy is not shown here, since it displays similar dispersoid characteristics to the 0.5Mn(L) and 1Mn(L) alloys.

The TEM images in Fig. 1d, e, and f show the Al(FeMn)Si dispersoids in the 0.5Mn(H), 0.5Mn(L), and 1Mn(L) alloys after extrusion, respectively. The dispersoids in the 0.5Mn(H) alloy remain significantly coarse ($\overline{D}$ ~ 187 nm) (see Fig. 1d and Table 3). The number density, N_v, and volume fraction, f_d, of the Al(FeMn)Si dispersoids in the 0.5Mn(H) alloy were measured to be ~4 μm^{-3} and 0.70%, respectively. Although a similar volume fraction of Al(FeMn)Si dispersoids is revealed in the 0.5Mn(L) alloy, their number density remains much higher than in the 0.5Mn(H) alloy (~317 μm^{-3} vs. ~4 μm^{-3}, respectively). The N_v and f_d of the dispersoids were comparably higher in the 0.7Mn(L) alloy than in the 0.5Mn(L) alloy, however, the N_v and f_d of the dispersoids in the 0.7Mn(L) and 1Mn(L) alloys were similar, approximately 416 μm^{-3} and 0.90%, respectively (see Table 3). Noticeably, the dispersoids experienced coarsening during extrusion as their average equivalent diameter increased from ~25 nm prior to extrusion (see Fig. 1b and c) to ~40 nm after extrusion (see Fig. 1e and f, and Table 3). According to Li et al. [18], the Al(FeMn)Si dispersoids become quite sensitive to coarsening at temperatures above 450 °C. Although the exposure time of the dispersoids to a high temperature, above 500 °C, during extrusion was quite limited owing to inductive heating and a relatively high ram speed (10 mm/s), the dispersoids still experienced moderate coarsening (Table 3). Indeed, solute diffusion is much faster during high-temperature extrusion owing to plastic deformation of the material, which accelerates coarsening of the Al(FeMn)Si dispersoids due to a high dislocation density. Furthermore, the dispersoids underwent morphological changes during extrusion. The platelet- and cuboidal- shaped dispersoids, observed in as-homogenized conditions (Fig. 1a, b and c), became more rounded after extrusion, making the dispersoids more oval or, to a lesser extent, spherical in shape (Fig. 1d, e and f). The mechanisms underlying these morphological changes will be the subject of a future work.

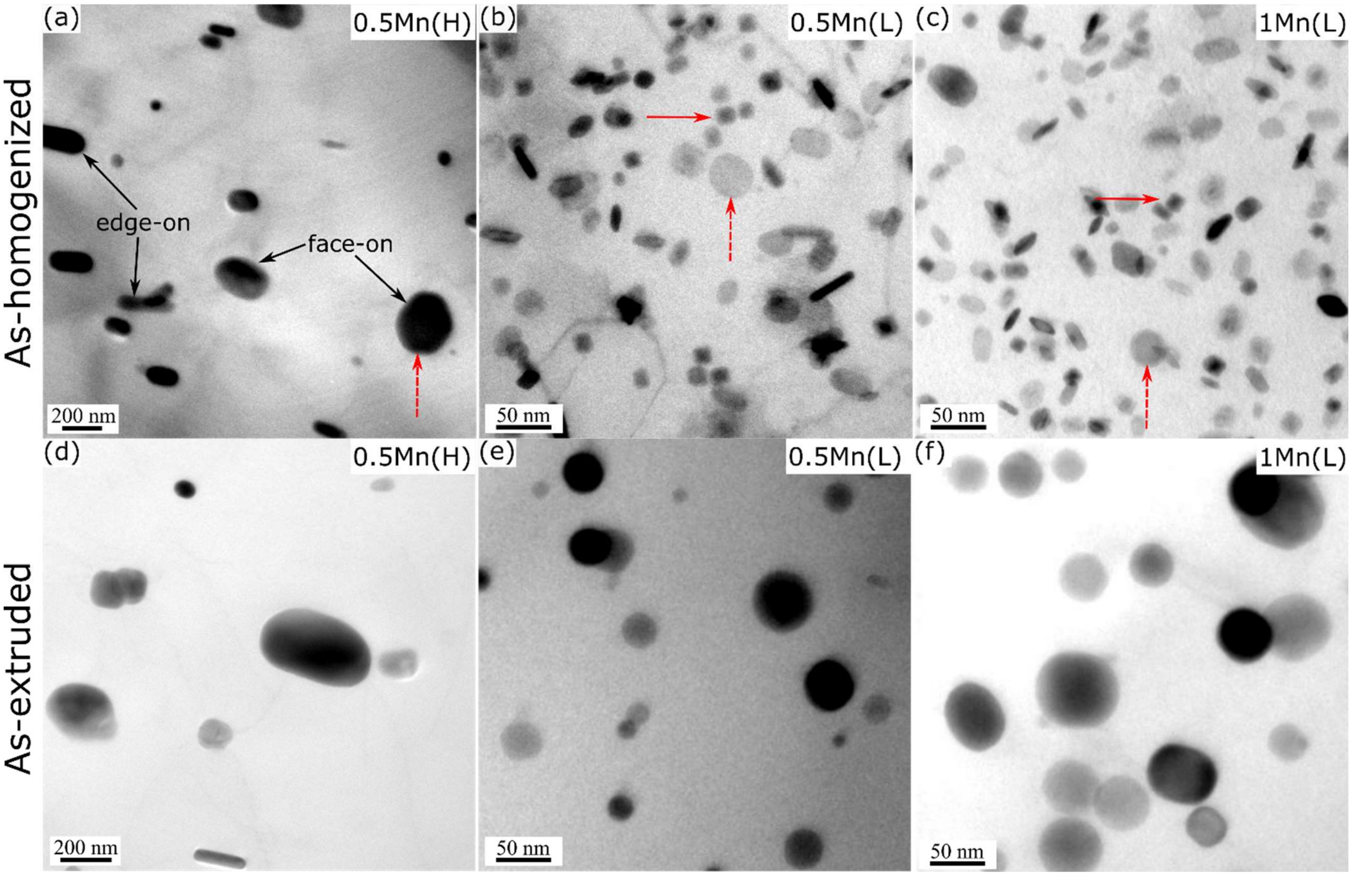

Fig. 1. Bright-field TEM images showing the Al(FeMn)Si dispersoids viewed along the $[001]_{Al}$ zone axis in the (a, d) 0.5Mn(H), (b, e) 0.5Mn(L) and (c, f) 1Mn(L) alloys before (a, b, c) and after (d, e, f) extrusion. Solid and dashed arrows indicate the cuboidal- and platelet-shaped dispersoids, respectively. Dispersoids positioned with their edges and broad surfaces (almost) normal to viewing direction are indicated as edge-on and face-on, respectively. Note that micrographs from 0.5Mn(H) alloy represent much larger area of α-Al matrix compared to those from 0.5Mn(L) and 1Mn(L) alloys.

Table 3. Quantitative TEM results of dispersoids in experimental alloys

Alloys	As-homogenized state			As-extruded state		
	$\overline{D}$, nm	N_v, μm^{-3}	f_d, %	$\overline{D}$, nm	N_v, μm^{-3}	f_d, %
0Mn	-	-	-	-	-	-
0.5Mn(H)	156.8 (±41)	4.3 (±3)	0.66 (±0.2)	187.5 (±52)	3.7 (±3)	0.70 (±0.2)
0.5Mn(L)	25.3 (±2.6)	971.5 (±112)	0.65 (±0.1)	40.3 (±2.5)	316.5 (±46)	0.64 (±0.1)
0.7Mn(L)	25.1 (±2.5)	1318.4 (±96)	0.85 (±0.1)	40.2 (±2.3)	415.4 (±36)	0.88 (±0.1)
1Mn(L)	25.2 (±2.7)	1383.1 (±121)	0.94 (±0.1)	40.2 (±2.5)	418.3 (±34)	0.93 (±0.1)

Fig. 2 shows the inverse pole figure (IPF) maps at the center of the extruded rods in the plane parallel to the extrusion direction. In the 0Mn alloy, the grains appear equiaxed and most of them have no substructure; the equivalent diameter of the grains is ~220 μm (Fig. 2a). This indicates that full recrystallization occurred during the extrusion of the base alloy [24]. In contrast, the grains in all the Mn-containing alloys are fibrous and aligned with the extrusion direction (Fig. 2b, c, and d). This implies that the dispersoids, owing to their Zener pinning effect, effectively retarded or inhibited recrystallization during extrusion in all the Mn-containing alloys [25]. The 0.5Mn(H) alloy contained a small portion of recrystallized grains (Fig. 2b). However, the presence of subgrain boundaries (misorientation angle ranging between 2° and 15°) in elongated grains suggests that the dynamic recovery mainly occurred during the extrusion of the 0.5Mn(H) alloy [26]. On the other hand, the grain structures of the alloys with fine and dense dispersoids (0.5Mn(L), 0.7Mn(L), and 1Mn(L)) were only partially recovered and contained mostly fibrous and un-recrystallized grains.

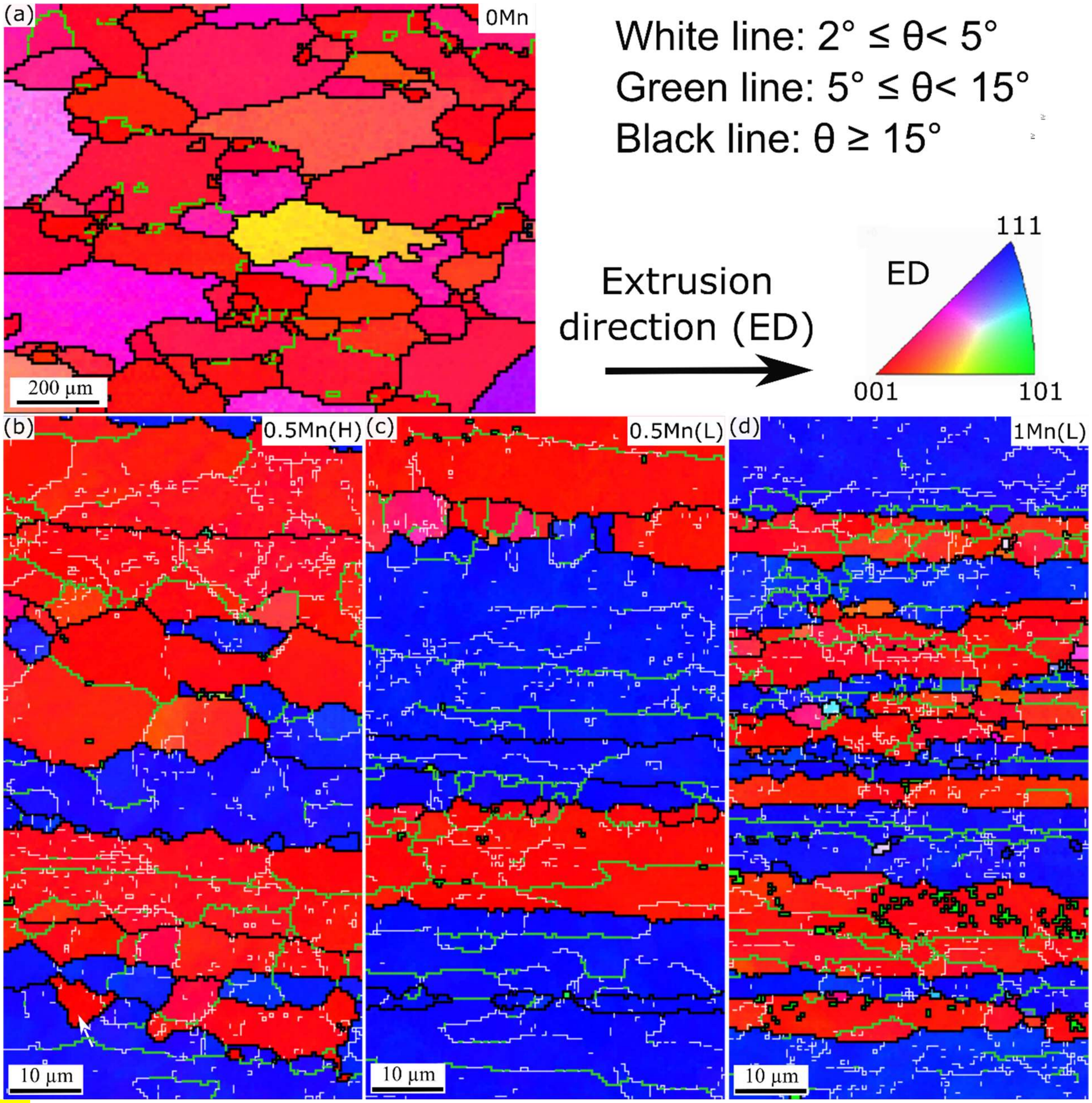

Fig. 2. EBSD (inverse pole figure) maps showing the as-extruded grain structures at the center of the extruded rods of (a) 0Mn, (b) 0.5Mn(H), (c) 0.5Mn(L) and (d) 1Mn(L) alloys in the plane parallel to the

extrusion direction (ED). The dashed arrows in Fig. 2b indicate the recrystallized grains. Note that the maps show the crystallographic orientations of grains along ED and the map from 0Mn alloy represent much larger area compared to those from 0.5Mn(H), 0.5Mn(L) and 1Mn(L) alloys.

Regarding the orientation of the grains, the IPF maps reveal that most of the grains in the 0Mn alloy exhibit $<001>_{Al}||$ED texture component (Fig. 2a), which is a typical recrystallization texture observed in the axisymmetrically deformed FCC materials [27]. In the Mn-containing alloys, which possess un-recrystallized grain structures, the grains are oriented along the extrusion axis in the <111> or <001> direction (Fig. 2b, c, and d). This confirms that the axisymmetric deformation that occurred during extrusion resulted in the evolution of the double-fiber texture comprising of <111> and <001> fibers [24, 28]. To reveal the effect of the fine and dense dispersoids on the texture and grain structure, the IPF maps of the cross sections of the extruded rods were acquired (Fig. 3); the measured area fractions of the <111> and <001> fiber textures and the average cross-sectional equivalent diameter of the grains are provided in Table 4. The ratio between the <111> and <001> fiber textures is equal to unity in the 0.5Mn(H) alloy, whereas the <111> fiber texture is more enhanced than the <001> fiber texture in the 0.5Mn(L) and 1Mn(L) alloys, accounting for approximately 70-72% of the grains (Table 4). Moreover, the average equivalent diameter of the grains in the 0.5Mn(L) and 1(Mn(L) alloys is noticeably reduced relative to that observed in the 0.5Mn(H) alloy (Table 4). The texture and grain structure differences observed in the 0.5Mn(L) and 1(Mn(L) alloys relative to the 0.5Mn(H) alloy are likely associated with the increased resistance of the material to plastic deformation during extrusion owing to the presence of fine and denser dispersoids in the former alloys [24].

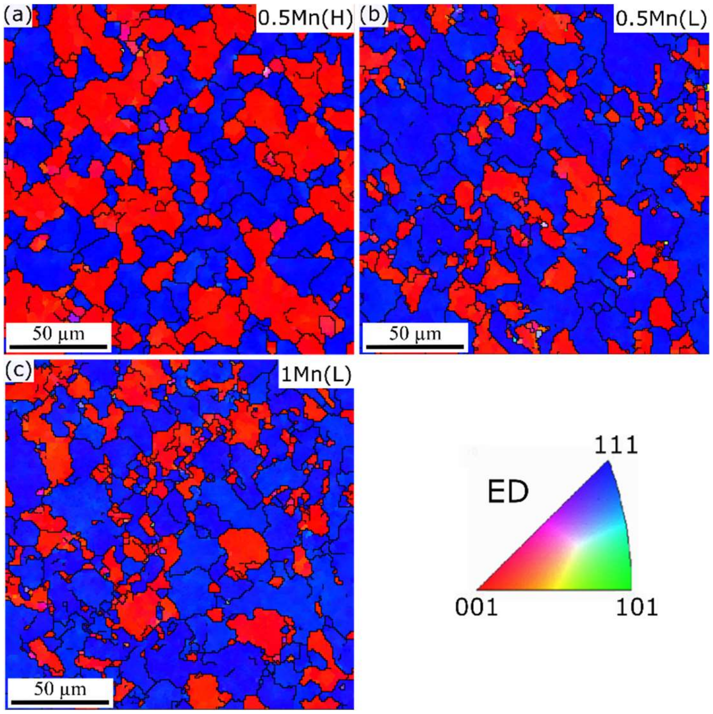

Fig. 3. EBSD (inverse pole figure) maps showing the as-extruded grain structures at the center of the extruded rods of (a) 0.5Mn(H), (b) 0.5Mn(L) and (c) 1Mn(L) alloys. Note that the images are captured from the planes perpendicular to the extrusion direction.

Table 4. Area fraction of <111> and <001> fibers and average equivalent diameter of grains obtained from EBSD maps in Fig. 3.

Alloys	Area fraction of <111> fibers, %	Area fraction of <001> fibers, %	Average eq. diameter of grains, μm
0.5Mn(H)	50	50	10.9
0.5Mn(L)	72	28	8.5
1Mn(L)	70	30	7.3

To obtain the best mechanical properties, it is important to dissolve the majority of the Mg_2Si particles in the aluminum matrix during extrusion for the subsequent T5 aging [29]. The as-extruded microstructures of the alloys, shown in Fig. 4, reveal the presence of few undissolved Mg_2Si particles in all alloys, confirming the effectiveness of the thermo-mechanical process during extrusion in dissolving the majority of Mg_2Si particles into the α-Al matrix. The area fraction of undissolved Mg_2Si particles was measured for all alloys and the results are listed in Table 5. More undissolved Mg_2Si particles were detected in 0Mn and 0.5Mn(H) alloys (~0.28%) compared to 0.5Mn(L), 0.7Mn(L) and 1Mn(L) alloys (~0.18%), which is also confirmed by their lower electrical conductivity of 0Mn and 0.5Mn(H) alloys.

Analysis of the extrusion process parameters, such as the exit temperature of the rods and the maximum pressure applied, indicate that the maximum pressures reached in the alloys with fine dispersoids are reasonably higher than that of the 0Mn and 0.5Mn(H) alloys with or without coarse dispersoids (Table 5). This confirms that the fine and dense dispersoids increased the resistance of the material to plastic deformation, which in turn caused a temperature increase during extrusion (Table 5). The combination of a higher degree of plastic deformation and a larger temperature increase, induced by the fine and dense dispersoids, caused the dissolution of relatively more constituent Mg_2Si particles into the matrix.

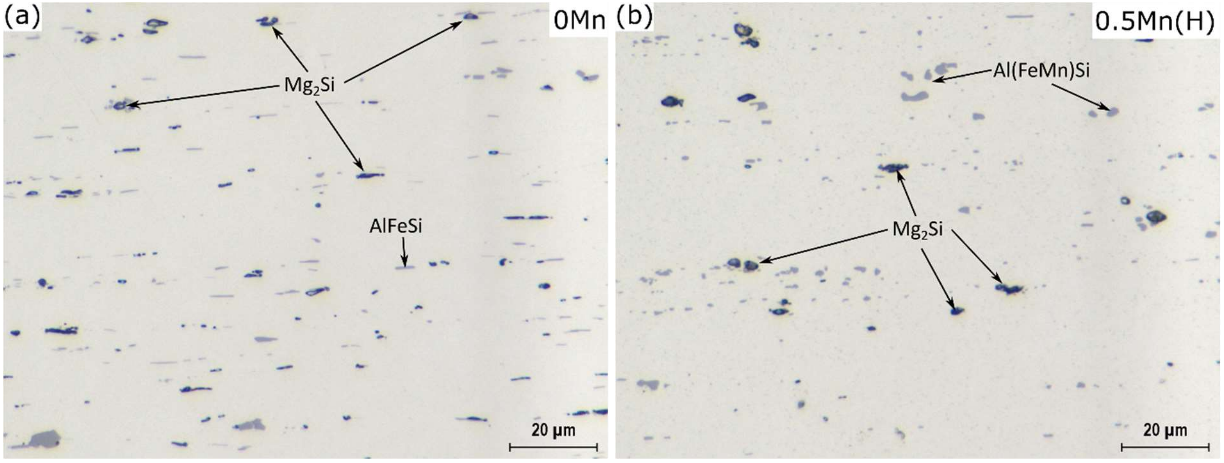

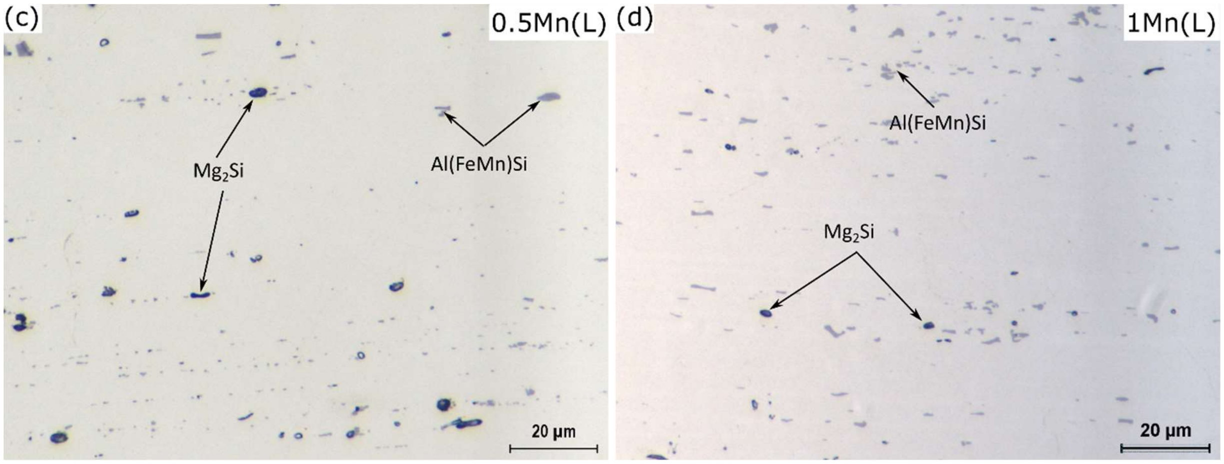

Fig. 4. Optical micrographs showing the as-extruded microstructures of the (a) 0Mn, (b) 0.5Mn(H), (c) 0.5Mn(L) and (d) 1Mn(L) alloys.

Table 5. The area % of Mg_2Si particles in as-extruded alloys, the exit temperature and the maximum pressure during extrusion and the electrical conductivity after extrusion for various alloys.

Alloys	**0Mn**	**0.5Mn(H)**	**0.5Mn(L)**	**0.7Mn(L)**	**1Mn(L)**
Area % of Mg_2Si	0.287	0.276	0.184	0.182	0.178
EC (%IACS)	43.4	42.5	37.8	36.6	37.6
Exit temperature, °C	535	534	557	558	555
Max. pressure, psi	1129	1252	1583	1640	1684

3.2 Mechanical properties and microstructure evaluation in the T5 condition

The aging curves of the various alloy conditions are shown in Fig. 5. An aging time of 0 h refers to the alloys in the as-extruded states, at which the 0.5Mn(L), 0.7Mn(L) and 1Mn(L) alloys have a higher hardness than the 0Mn and 0.5Mn(H) alloys, mostly due to the combination of the presence of fine dispersoids and higher Mg and Si solute levels. All Mn-containing alloys reached peak ageing in 5 h, as opposed to 8 h in the case of the 0Mn alloy. The aging kinetics of the alloys with deformed grain structures, which are all Mn-containing alloys in the present study, are reported to accelerate owing to much faster solute diffusion compared to the alloy (0Mn) containing a recrystallized grain structure [30]. At the peak-aging stage, the 0.5Mn(L) alloy displays higher hardness than the 0.5Mn(H) alloy (~116 vs ~112 HV). Moreover, comparing the hardness of the Mn-containing alloys at the peak and over aging stages, a higher Mn content in the alloy leads to a lower hardness (Fig. 5). The reason for these differences is discussed further on in this section.

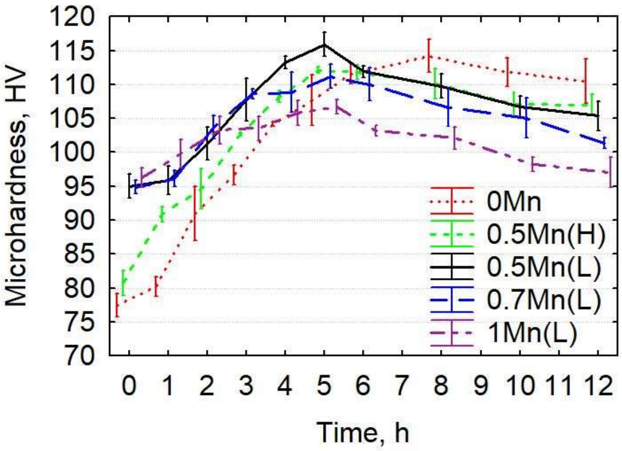

Fig. 5. Microhardness evolution of extruded alloys as a function of aging time at 180 °C. Note that 0 h refers to the as-extruded state of the alloys.

The mechanical properties of the alloys were determined at 180 °C for 5 h, which corresponds to the peak aging of the Mn-containing alloys. Consistent with the hardness results (Fig. 5), the 0.5Mn(L) alloy exhibits the highest compressive YS (~335 MPa) among all the experimental alloys under T5 (see Fig. 6a). Comparatively, the compressive YS of the 0.5Mn(H) alloy is ~318 MPa, which is still much higher than that of the base 0Mn alloy (~270 MPa). Noticeably, the compressive YSs of the Mn-containing alloys showed a tendency to decline with increasing Mn content, decreasing from 335 MPa in the 0.5Mn(L) alloy to 310 MPa in the 0.7Mn(L) alloy, and further to 290 MPa in the 1Mn(L) alloy (Fig. 6a). For comparison, the tensile properties under the same T5 conditions were also measured, and the results are shown in Fig. 6b. Although minor differences exist between compressive and tensile YSs, which can be due to different loading paths applied, a similar trend is observed. The YS and ultimate tensile strength (UTS) for the base 0Mn alloy are 260 MPa and 294 MPa, respectively, while those of the 0.5Mn(H) alloy are 312 MPa and 335 MPa, respectively. The tensile strengths of the 0.5Mn(L) alloy are also the highest (336 MPa in YS and 360 MPa in UTS) among all the alloys. Moreover, the YS and UTS values still showed a tendency to decline with increasing Mn content among the 0.5Mn(L), 0.7Mn(L), and 1Mn(L) alloys (Fig. 6b).

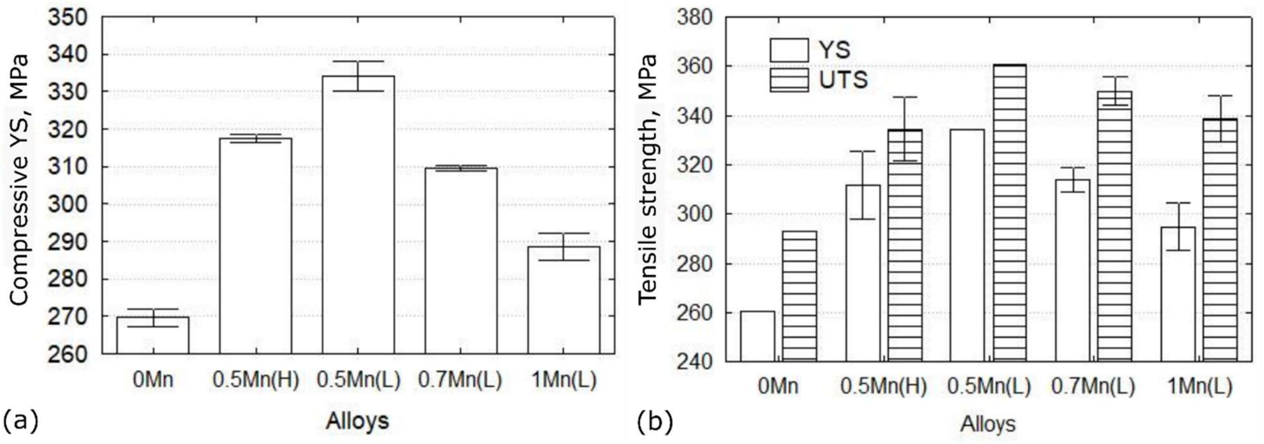

Fig. 6. (a) Compressive YSs and (b) tensile strengths of all extruded alloys in the T5 condition.

The general precipitation sequence of the Al-Mg-Si 6xxx alloy has been described as follows: supersaturated solid solution → GP zones → metastable β'' → metastable β′ → equilibrium β-Mg_2Si precipitates [31]. The precipitation of β'' in the Al-Mg-Si alloys has been the subject of multiple studies since the largest strengthening contribution of peak-hardening is derived from this phase [32, 33]. The precipitation microstructures in the experimental alloys were investigated using TEM (Fig. 7). In the 0Mn alloy, the precipitates are uniformly distributed and quite fine, with an average cross-sectional diameter of 3.6 nm and a length of 27 nm (Fig. 7a and Table 6). Precipitates with these dimensions have been identified as the β'' phase [31]. The TEM image of the 0.5Mn(H) alloy (Fig. 7b) shows that the β'' precipitates are longer than those observed in the 0Mn alloy (31 nm vs. 27 nm), however, their diameters are almost identical to the precipitates observed in the 0Mn alloy (see Table 6). Moreover, the number density of the β'' precipitates is reasonably higher in the 0.5Mn(H) alloy compared to the 0Mn alloy ($19.9 \cdot 10^{-6}$ nm^{-3} vs $13.6 \cdot 10^{-6}$ nm^{-3}). The longer and higher number of β'' precipitates reduces the interparticle spacing, thus increasing the strengthening effect on the alloy (Fig. 6) [30]. Faster growth of the β'' precipitates in the 0.5Mn(H) alloy is the result of faster solute diffusion due to its deformed grain structure as opposed to the recrystallized structure in the 0Mn alloy (Fig. 2) [30]. Moreover, the fibrous and partially recovered grain structure of the 0.5Mn(H) alloy provides an additional strengthening contribution to the alloy, to a certain extent, owing to the presence of subgrain and dislocation strengthening [30].

The microstructure of the 0.5Mn(L) alloy is predominantly composed of β'' precipitates and fine Al(FeMn)Si dispersoids (Fig. 7c). In addition, coarser MgSi precipitates are observed, exclusively appearing adjacent to the Al(FeMn)Si dispersoids, which were identified as the β' phase based on their size and morphology [34, 35]. The Al(FeMn)Si dispersoids are known to favor the precipitation of β' by acting as preferential nucleation sites [34, 35], making the Al-Mg-Si alloys more quench-sensitive [35]. However, the TEM analyses of the as-extruded alloys revealed no evidence of the presence of the β' precipitates in the α-Al matrices (see Fig. 1d,e,f). This indicates that the water quenching of extrudates at the exit from the die provided sufficiently high cooling rate that effectively suppressed the precipitation of β' during cooling stage. It is therefore undoubted that the β' precipitates, appearing in the microstructures of the alloys in the T5 condition (Fig. 7c,d,e), formed during ageing stage by nucleating on the pre-existing Al(FeMn)Si dispersoids. The average diameter and average length of the β' precipitates were measured as 15 nm and 75 nm, respectively. Although fine dispersoids promote the precipitation of β' at the expense of β'' in the 0.5Mn(L) alloy, the number density of the β'' precipitates remain high ($16.1 \cdot 10^{-6}$ nm^{-3}), since the amount of dissolved constituent Mg_2Si particles in the α-Al matrix during extrusion is higher in the 0.5Mn(L) alloy than in the 0Mn and 0.5Mn(H) alloys (Fig. 4 and Table 5). Moreover, the β'' precipitates in the 0.5Mn(L) alloy have a larger average diameter than those in the 0.5Mn(H) alloy (3.5 nm vs. 4.3 nm) (see Table 6). Some MgSi precipitates tend to form along the dislocations (see Fig. 7c); this behavior is occasionally observed in all Mn-containing alloys. As for the strength evolution under T5, the combined presence of a large amount of β'', relatively lower amount of β' precipitates, and the Al(FeMn)Si dispersoids moderately increases the strength of the 0.5Mn(L) alloy relative to the 0.5Mn(H) alloy (Fig. 6).

The nature of the β'' and β' precipitation in the 0.7Mn(L) (Fig. 7d) and 1Mn(L) (Fig. 7e) alloys is similar to that of the 0.5Mn(L) alloy. However, with increasing Mn content, the number density of the β'' precipitates tends to decrease remarkably from $16.1\cdot10^{-6}$ nm^{-3} in the 0.5Mn(L) alloy to $13.1\cdot10^{-6}$ nm^{-3} in the 0.7Mn(L) alloy, and further to $9.0\cdot10^{-6}$ nm^{-3} in the 1Mn(L) alloy (Table 6). Indeed, both the microhardness at peak-aging and YS of the AA6082 alloy tends to decrease with an increase in Mn content (Fig. 5 and Fig. 6). The YSs of the experimental alloys are largely governed by the β'' precipitates. The strengthening effect of fine dispersoids in the 0.5Mn(L), 0.7Mn(L), and 1Mn(L) alloys under T5 is only complementary as the strength increment due to dispersoids in the alloy is not in a linear manner, owing to their overlapping with the β'' and β' precipitates [36].

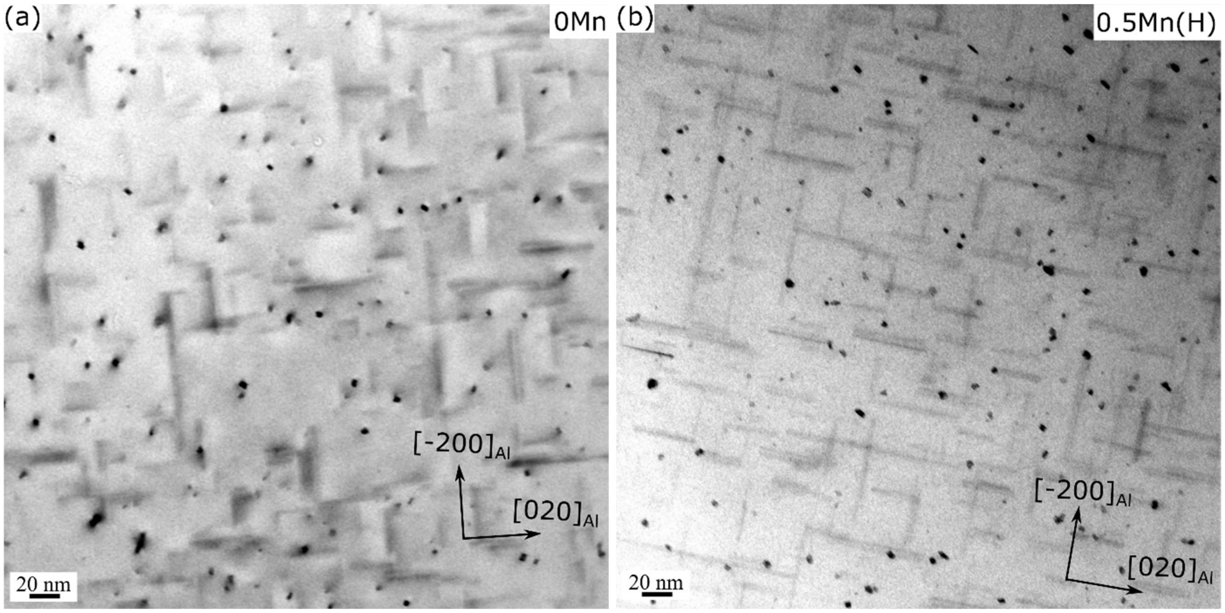

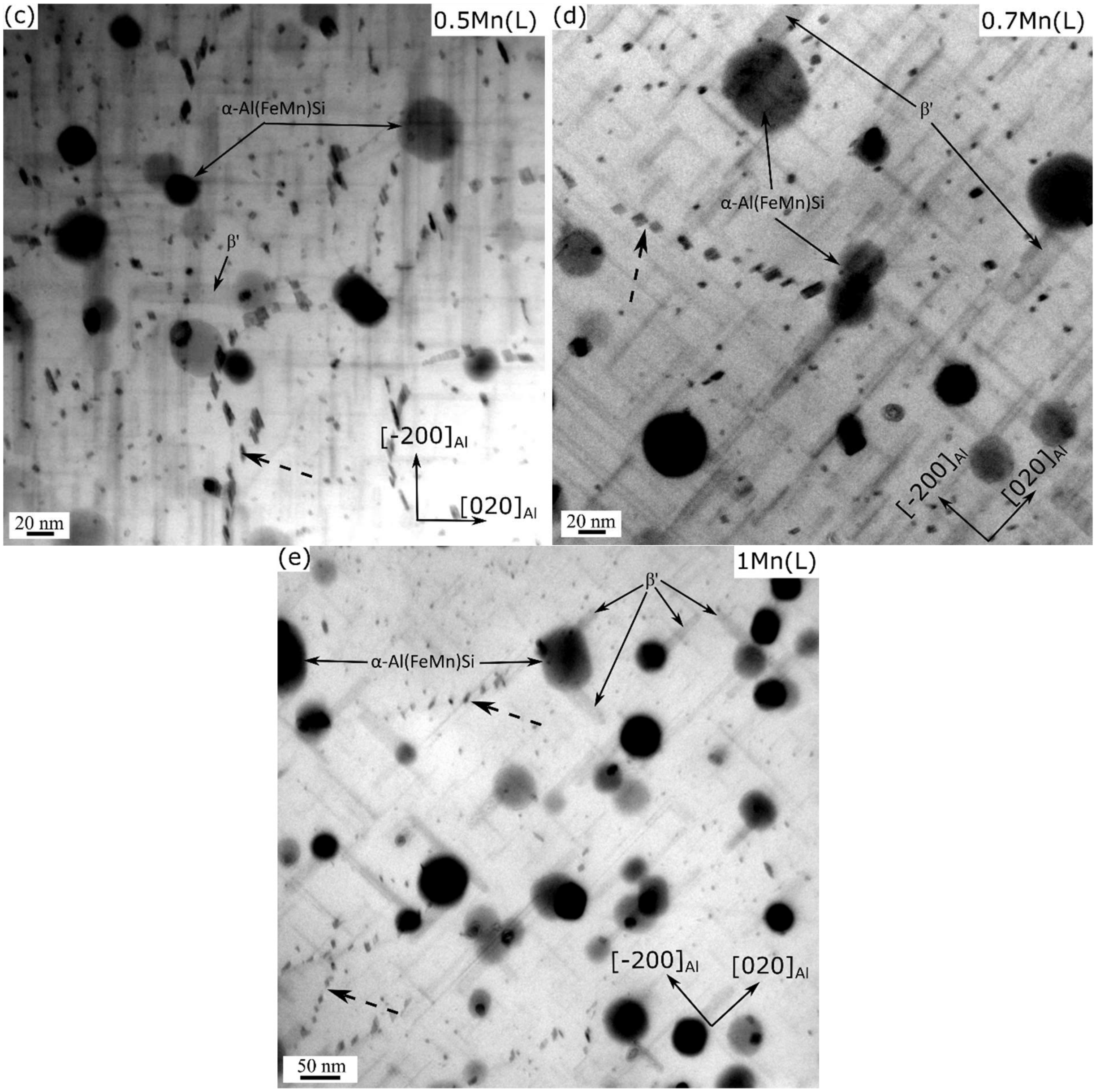

Fig. 7. Bright-field TEM images showing the precipitates in (a) 0Mn, (b) 0.5Mn(H), (c) 0.5Mn(L), (d) 0.7Mn(L) and (e) 1Mn(L) alloys in the T5 condition. Dashed arrows indicate the precipitates formed along dislocations.

Table 6. Quantitative TEM results of β"; cross-sectional diameter (d), length (l) and number density (N_v) of the experimental alloys in the T5 condition.

Alloy	d, nm	l, nm	N_v, nm^{-3}
0Mn	3.6 (±0.9)	27 (±6)	$13.6 \cdot 10^{-6}$
0.5Mn(H)	3.5 (±0.9)	31.1 (±7)	$19.9 \cdot 10^{-6}$
0.5Mn(L)	4.3 (±1.0)	32.5 (±12)	$16.1 \cdot 10^{-6}$
0.7Mn(L)	4.3 (±0.9)	34.2 (±7)	$13.1 \cdot 10^{-6}$
1Mn(L)	4.5 (±1.0)	32.1 (±13)	$9.0 \cdot 10^{-6}$

In the as-extruded 0.5Mn(L), 0.7Mn(L), and 1Mn(L) alloys, the majority of Si atoms were dissolved in the α-Al matrix, since almost all the constituent Mg_2Si particles experienced dissolution during extrusion. However, some of the Si is also bound to the Al(FeMn)Si intermetallics and dispersoids formed during solidification and homogenization, respectively. To estimate the amount of Si consumed by the Al(FeMn)Si phase (intermetallics and dispersoids combined) in the 0.5Mn(L), 0.7Mn(L), and 1Mn(L) alloys, thermodynamic equilibrium analysis was performed using Thermo-Calc software to calculate the volume fraction, f_d, and wt.% of the Al(FeMn)Si phase at 400 °C, at which the alloys were homogenized (Table 7). It is assumed that all excess Mn in the α-Al matrix becomes bound to Al(FeMn)Si dispersoids during homogenization, and the Al(FeMn)Si intermetallics/dispersoids remain insoluble during extrusion. In general, the estimated f_d of the Al(FeMn)Si phase vs. the experimentally measured f_d values was approximately 1.9% vs. 1.8% for the 0.5Mn(L) alloy and 3.0% vs. 3.1% for the 1Mn(L) alloy, indicating a reasonable accuracy of the thermodynamic analyses in estimating the consumed Si content. As listed in Table 7, the estimated content of Si consumed by the Al(FeMn)Si phase increases from 0.25 wt.% in the 0.5Mn(L) alloy to 0.33 wt.% in the 0.7Mn(L) alloy, and further to 0.44 wt.% in the 1Mn(L) alloy. Owing to the Mg/Si ratio of approximately unity in β'' [37, 38], the reduced Si concentration in the α-Al matrix with a higher Mn level becomes the primary reason for the reduction in the number density of β'', which, in turn, leads to the degradation of the YS. Moreover, increasing the Mn content of the alloys, increased the number density of the Al(FeMn)Si dispersoids (Table 3). More dispersoids, in turn, promoted the precipitation of less favorable β' precipitates at the expense of β'' during aging, thus leading to the strength degradation of the alloys containing higher Mn concentrations under T5, to a certain extent.

Table 7. The f_d and wt.% of the Al(FeMn)Si phase as well as the consumed content of Si, estimated by thermodynamic equilibrium analysis at 400 ºC.

Alloys	f_d of Al(FeMn)Si phase, %	Wt.% of Al(FeMn)Si phase, %	Wt.% of Si consumed by Al(FeMn)Si phase
0.5Mn(L)	1.8	2.4	0.25
0.7Mn(L)	2.3	3.1	0.33
1Mn(L)	3.0	4.1	0.44

3.3 Mechanical responses and microstructure evaluation during thermal exposure

The elevated-temperature mechanical properties of the Al–Mg–Si and Al-Mn-Mg alloys can be significantly enhanced through the introduction of thermally stable α-Al(MnFe)Si dispersoids [10,11,12,15], which affect hot workability as well as microstructural stability during high-temperature thermal exposure. To investigate how the dispersoids improved the mechanical performance during thermal exposure, the T5-treated alloys were further exposed to 300 °C for 100 h, followed by conducting compressive YS tests at 20 and 300 °C. As shown in Fig. 8a, the YS of the 0Mn alloy at room temperature is ~55 MPa, whereas the 0.5Mn(H) alloy displays a YS of ~65 MPa. In contrast, the alloys with fine and dense dispersoids (0.5Mn(L), 0.7Mn(L), and 1Mn(L) alloys) exhibit improved ambient-temperature YS, ranging between 100 and 110 MPa. The 0.7Mn(L) and 1Mn(L) alloys possess higher YSs than the 0.5Mn(L) alloy by ~10 MPa.

As for the elevated-temperature strength at 300 °C (Fig. 8b), both 0Mn and 0.5Mn(H) alloys exhibit approximately the same YS (~36 MPa), while the alloys with fine and dense dispersoids display much higher YSs, ranging from 55 to 60 MPa. The YS increases in the 0.5Mn(L) and 1Mn(L) alloys relative to the 0Mn and 0.5Mn(H) alloys are 19 MPa (~55%) and 24 MPa (~70%), respectively, indicating the high efficacy of fine and dense Al(FeMn)Si dispersoids to improve the elevated-temperature strengths of aluminum alloys.

TEM microstructural analysis of the alloys after thermal exposure at 300 °C for 100 h revealed that the β'' and β' precipitates present in the T5 condition (Fig. 7) underwent a complete transformation into coarse equilibrium Mg_2Si particles (see Fig. 9a and d) owing to their high sensitivity to temperature [3]. The complete loss of the strengthening effect of the β'' and β' precipitates is responsible for the significant strength reduction in all the experimental alloys (Fig. 8a) relative to the T5 state (Fig. 6). The fine and dense dispersoids (Fig. 9 and Table 8), on the contrary, showed no coarsening tendency during thermal exposure displaying the same size range as that in the as-extruded (Fig. 1e and f and Table 3) or T5-treated alloys (Fig. 7d, e, and f). This indicates the effective resistance of dispersoids to coarsening at 300 °C [11].

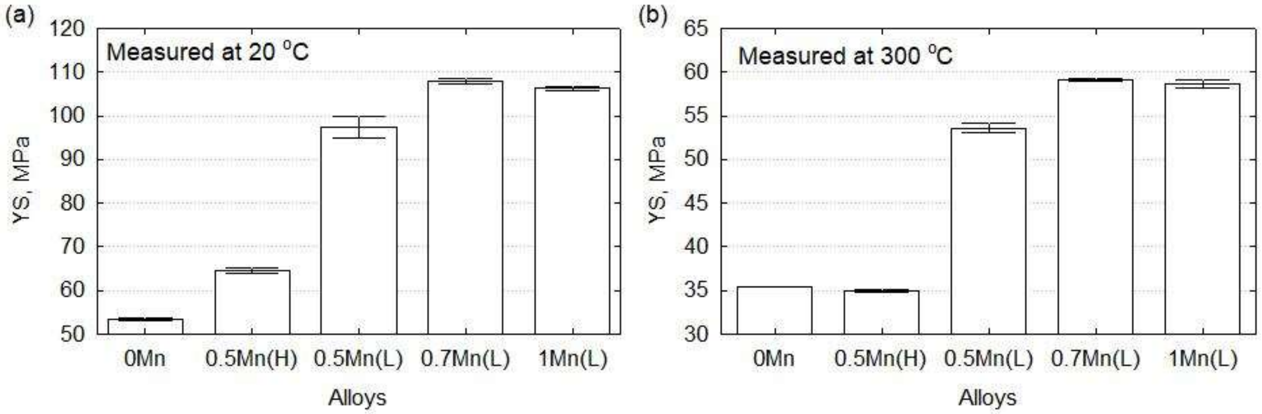

Fig. 8. The YSs of the experimental alloys exposed to 300 °C for 100 h, tested at (a) 20 and (b) 300 °C.

In the absence of the β''/β' precipitate strengthening effect, the YS increments caused by dispersoids at ambient temperature can generally be predicted using the Orowan bypass equation [3], in assuming that the solid solution strengthening and grain boundary strengthening are more or less similar in all the experimental alloys.

$$\Delta\sigma_{or} = \frac{0.84MGb}{2\pi(1-\nu)^{1/2}\lambda} ln\frac{r_d}{b} \qquad (7)$$

where, r_d is the equivalent radius of the dispersoids, λ is interparticle spacing $\left(\lambda = r_d \cdot \left(\frac{2\pi}{3f_d}\right)^{1/2}\right)$, ν is Poisson's ratio $(\nu = 0.3)$, and f_d is the volume fraction of the dispersoids. The predicted strength increments are compared to the experimentally measured values in Table 8. The experimentally measured ambient-temperature YS increments due to the dispersoids in 0.5Mn(H), 0.5Mn(L), 0.7Mn(L) and 1Mn(L) alloys relative to the 0Mn alloy were 10 MPa, 43 MPa, 53 MPa and 51 MPa, respectively. Indeed, there is excellent agreement between the predicted and measured YS increments, confirming that dispersoid bypassing by dislocation looping (i.e., Orowan) is the main operative strengthening mechanism in the experimental alloys after thermal exposure. There is not yet a reliable constitutive equation for the approximation of elevated-temperature strengths in aluminum alloys.

It is also noteworthy that the higher Mn content in the 0.7Mn(L) alloy compared to the 0.5Mn(L) alloy induced the formation of a relatively higher fraction of dispersoids (see Table 3), thus providing a relatively higher strengthening effect on the alloy (see Fig. 8). An even higher Mn content in the 1Mn(L) alloy showed no further increase in the strengthening effect (see Fig. 8), since the addition of Mn at this level mainly contributed to the increased fraction of Al(FeMn)Si intermetallics. Therefore, a significant improvement in both the ambient- and elevated-temperature strengths of extruded AA6082-T5 alloys during high-temperature thermal exposure enables the broader usage of these alloys in more critical automotive and aerospace applications, which is achieved through the incorporation of a large number of fine and thermally stable dispersoids into its microstructure by the addition of 0.5-0.7 wt.% Mn and proper heat treatment (400 °C/5 h).

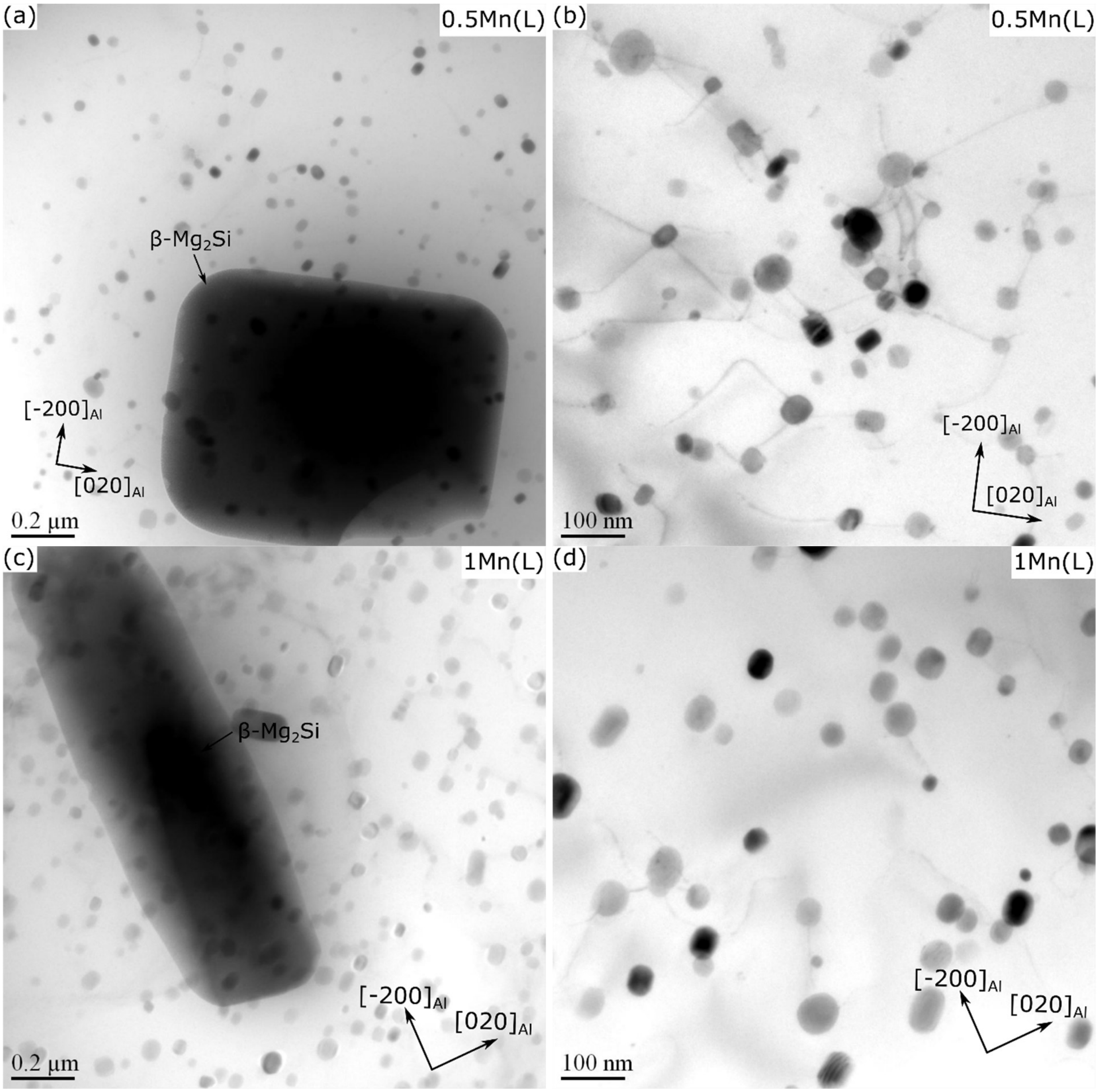

Fig. 9. Bright-field TEM images showing the precipitates in the α-Al matrix of the (a, b) 0.5Mn(L) and (c, d) 1Mn(L) alloys exposed to 300 °C for 100 h.

Table 8. Quantitative TEM results of dispersoids in experimental alloys exposed to 300 °C for 100 h.

Alloys	$\overline{D}$, nm	N_v, μm^{-3}	f_d, %
0Mn	-	-	-
0.5Mn(H)	174.5 (±32.0)	3.7 (±2.1)	0.70 (±0.9)
0.5Mn(L)	38.1 (±2.0)	353.9 (±62)	0.64 (±0.16)
0.7Mn(L)	42.2 (±2.9)	415.4 (±39)	0.89 (±0.13)
1Mn(L)	43.1 (±2.7)	418.3 (±41)	0.94 (±0.14)

Table 9. Predicted and experimentally measured ambient-temperature YS increments due to dispersoids* in all the experimental alloys.

Alloys	0Mn	0.5Mn(H)	0.5Mn(L)	0.7Mn(L)	1Mn(L)
$\Delta\sigma_{or}$, MPa	0	12	43.5	51	51.5
Experimental, MPa	0	10	43	53	51

* The quantitative characteristics of Al(FeMn)Si dispersoids are given in Table 8.

4. Conclusions

- The new low-temperature homogenization treatment (400 °C/5 h) for Al-Mg-Si AA6082 alloys resulted in the precipitation of a high density of Al(FeMn)Si dispersoids as opposed to a lower density of coarse dispersoids formed during conventional industrial homogenization (550 °C/5 h).
- Increasing the density of fine dispersoids increased the material's resistance to plastic deformation. This, in turn, resulted in a higher extrusion exit temperature, allowing the dissolution of more constituent Mg_2Si particles into the α-Al matrix during extrusion.
- Full recrystallization occurred during the extrusion of the Mn-free alloy. The presence of dispersoids effectively retarded or inhibited recrystallization during extrusion. A high density of fine dispersoids promoted the evolution of the <111> texture component at the expense of the <001> texture during extrusion.
- The co-existence of a large volume of β'', smaller amount of β' precipitates, and fine dispersoids rendered the alloy with 0.5% Mn a substantial increase in ambient temperature yield strength of 65-75 MPa under the T5 condition compared to the base alloy without dispersoids. With a further increase in the Mn content up to 1.0%, the ambient-temperature strengths of the AA6082 alloys showed a decline, which is attributed to the decreasing number density of β'' precipitates.
- Thermal exposure at 300 °C for 100 h transformed the β''/β' precipitates to the equilibrium β phase, thereby abolishing the strength contribution from precipitation hardening. However, the fine and dense dispersoids remained stable and became the principal strengthening contributor, leading to a 55-70% increase in the elevated-temperature YS at 300 °C relative to the alloys either without dispersoids or with a low density of coarse dispersoids.
- The optimum dispersoid strengthening effect after thermal exposure was obtained with 0.7% Mn. A further increase in Mn content to 1.0%, however, had no additional contribution to the alloy strength as it mainly increased the fraction of Mn-containing intermetallics that formed during solidification.

Acknowledgements

The authors would like to acknowledge the financial support of the Natural Sciences and Engineering Research Council of Canada (NSERC) under the Grant No. CRDPJ 514651-17 and Rio Tinto Aluminum through the Research Chair in the Metallurgy of Aluminum Transformation at University of Quebec in Chicoutimi.

References

[1] S. Kumar, P.S. Grant, K.A.Q. O'Reilly, Evolution of Fe Bearing Intermetallics During DC Casting and Homogenization of an Al-Mg-Si Al Alloy, Metall. Mater. Trans. A, 47A (2016) 3000-3014.
[2] R. Hu, T. Ogura, H. Tezuka, T. Sato, Q. Liu, Dispersoid Formation and Recrystallization Behavior in an Al-Mg-Si-Mn Alloy, Journal of Materials Science & Technology, 26 (2010) 237-243.
[3] F. Qian, S.B. Jin, G. Sha, Y.J. Li, Enhanced dispersoid precipitation and dispersion strengthening in an Al alloy by microalloying with Cd, Acta Mater., 157 (2018) 114-125.
[4] Q. Du, W.J. Poole, M.A. Wells, N.C. Parson, Microstructure evolution during homogenization of Al-Mn-Fe-Si alloys: Modeling and experimental results, Acta Mater., 61 (2013) 4961-4973.
[5] K. Tang, Q. Du, Y.J. Li, Modelling microstructure evolution during casting, homogenization and ageing heat treatment of Al-Mg-Si-Cu-Fe-Mn alloys, Calphad-Computer Coupling of Phase Diagrams and Thermochemistry, 63 (2018) 164-184.
[6] A.M.F. Muggerud, E.A. Mørtsell, Y. Li, R. Holmestad, Dispersoid strengthening in AA3xxx alloys with varying Mn and Si content during annealing at low temperatures, Materials Science and Engineering: A, 567 (2013) 21-28.
[7] A.R. Farkoosh, X. Grant Chen, M. Pekguleryuz, Dispersoid strengthening of a high temperature Al-Si-Cu-Mg alloy via Mo addition, Mater. Sci. Eng., A, 620 (2014) 181-189.
[8] A.R. Farkoosh, X. Grant Chen, M. Pekguleryuz, Interaction between molybdenum and manganese to form effective dispersoids in an Al-Si-Cu-Mg alloy and their influence on creep resistance, Mater. Sci. Eng., A, 627 (2015) 127-138.
[9] L. Jin, K. Liu, X.G. Chen, Evolution of dispersoids and their effects on elevated-temperature strength and creep resistance in Al-Si-Cu 319 cast alloys with Mn and Mo additions, Materials Science and Engineering: A, 770 (2020) 138554.
[10] K. Liu, X.G. Chen, Development of Al–Mn–Mg 3004 alloy for applications at elevated temperature via dispersoid strengthening, Mater Design, 84 (2015) 340-350.
[11] K. Liu, H. Ma, X.G. Chen, Enhanced elevated-temperature properties via Mo addition in Al-Mn-Mg 3004 alloy, J. Alloys Compd., 694 (2017) 354-365.
[12] K. Liu, X.G. Chen, Evolution of Intermetallics, Dispersoids, and Elevated Temperature Properties at Various Fe Contents in Al-Mn-Mg 3004 Alloys, Metall Mater Trans B, 47 (2016) 3291-3300.
[13] Z. Li, Z. Zhang, X.G. Chen, Microstructure, elevated-temperature mechanical properties and creep resistance of dispersoid-strengthened Al-Mn-Mg 3xxx alloys with varying Mg and Si contents, Mater. Sci. Eng., A, 708 (2017) 383-394.
[14] J. Rakhmonov, K. Liu, L. Pan, F. Breton, X.G. Chen, Enhanced mechanical properties of high-temperature-resistant Al–Cu cast alloy by microalloying with Mg, J. Alloys Compd., 827 (2020) 154305.
[15] G.S. Wang, K. Liu, S.L. Wang, Evolution of Elevated-Temperature Strength and Creep Resistance during Multi-Step Heat Treatments in Al-Mn-Mg Alloy, Materials, 11 (2018).
[16] K. Liu, X.G. Chen, Influence of heat treatment and its sequence on elevated-temperature properties of Al-Mn-Mg 3004 alloy, Mater. Sci. Eng., A, 697 (2017) 141-148.
[17] J. Rakhmonov, G. Timelli, A. Fabrizi, F. Bonollo, Effect of V and Zr microalloying, and heat treatment on microstructure and mechanical properties of secondary Al-7Si-3Cu-0.3Mg alloy, International Journal of Materials Research, 109 (2018) 1099-1112.

[18] C. Li, K. Liu, X.G. Chen, Improvement of elevated-temperature strength and recrystallization resistance via Mn-containing dispersoid strengthening in Al-Mg-Si 6082 alloys, Journal of Materials Science & Technology, 39 (2020) 135-143.
[19] X. Qian, N. Parson, X.G. Chen, Effects of Mn addition and related Mn-containing dispersoids on the hot deformation behavior of 6082 aluminum alloys, Materials Science and Engineering: A, 764 (2019) 138253.
[20] S.M. Allen, Foil thickness measurements from convergent-beam diffraction patterns, Philos. Mag. A, 43 (1981) 325-335.
[21] Y.J. Li, L. Arnberg, Quantitative study on the precipitation behavior of dispersoids in DC-cast AA3003 alloy during heating and homogenization, Acta Mater., 51 (2003) 3415-3428.
[22] O. Engler, C.D. Marioara, Y. Aruga, M. Kozuka, O.R. Myhr, Effect of natural ageing or pre-ageing on the evolution of precipitate structure and strength during age hardening of Al–Mg–Si alloy AA 6016, Materials Science and Engineering: A, 759 (2019) 520-529.
[23] A. De Luca, S. Shu, D.N. Seidman, Effect of microadditions of Mn and Mo on dual L12- and α-precipitation in a dilute Al-Zr-Sc-Er-Si alloy, Mater. Charact., 169 (2020) 110585.
[24] J.Q. Chen, W.J. Poole, N.C. Parson, The effect of through thickness texture variation on the anisotropic mechanical response of an extruded Al-Mn-Fe-Si alloy, Mater. Sci. Eng., A, 730 (2018) 24-35.
[25] K. Huang, K. Zhang, K. Marthinsen, R.E. Loge, Controlling grain structure and texture in Al-Mn from the competition between precipitation and recrystallization, Acta Mater., 141 (2017) 360-373.
[26] Y. Mahmoodkhani, M.A. Wells, W.J. Poole, L. Grajales, N. Parson, The Development of Grain Structure During Axisymmetric Extrusion of AA3003 Aluminum Alloys, Metall. Mater. Trans. A, 46A (2015) 5920-5932.
[27] S.Y. Kim, C.H. Choi, D.N. Lee, Deformation and Annealing Textures of Drawn Aluminum Bronze Wires, Mater. Sci. Forum, 408-412 (2002) 913-918.
[28] S. Kaneko, K. Murakami, T. Sakai, Effect of the extrusion conditions on microstructure evolution of the extruded Al-Mg-Si-Cu alloy rods, Mater. Sci. Eng., A, 500 (2009) 8-15.
[29] Y. Birol, The effect of processing and Mn content on the T5 and T6 properties of AA6082 profiles, J. Mater. Process. Technol., 173 (2006) 84-91.
[30] C. Sigli, F. De Geuser, A. Deschamps, J. Lepinoux, M. Perez, Recent advances in the metallurgy of aluminum alloys. Part II: Age hardening, Cr Phys, 19 (2018) 688-709.
[31] G.A. Edwards, K. Stiller, G.L. Dunlop, M.J. Couper, The precipitation sequence in Al-Mg-Si alloys, Acta Mater., 46 (1998) 3893-3904.
[32] A.K. Gupta, D.J. Lloyd, S.A. Court, Precipitation hardening in Al-Mg-Si alloys with and without excess Si, Mater. Sci. Eng., A, 316 (2001) 11-17.
[33] S. Roy, L.F. Allard, A. Rodriguez, W.D. Porter, A. Shyam, Comparative Evaluation of Cast Aluminum Alloys for Automotive Cylinder Heads: Part II-Mechanical and Thermal Properties, Metall. Mater. Trans. A, 48A (2017) 2543-2562.
[34] K. Strobel, M.A. Easton, M.D.H. Lay, P.A. Rometsch, S. Zhu, L. Sweet, N.C. Parson, A.J. Hill, Quench Sensitivity in a Dispersoid-Containing Al-Mg-Si Alloy, Metall. Mater. Trans. A, 50a (2019) 1957-1969.
[35] B. Milkereit, M.J. Starink, P.A. Rometsch, C. Schick, O. Kessler, Review of the Quench Sensitivity of Aluminium Alloys: Analysis of the Kinetics and Nature of Quench-Induced Precipitation, Materials, 12 (2019).
[36] A. de Vaucorbeil, W.J. Poole, C.W. Sinclair, The superposition of strengthening contributions in engineering alloys, Mater. Sci. Eng., A, 582 (2013) 147-154.
[37] H.W. Zandbergen, S.J. Andersen, J. Jansen, Structure Determination of Mg₅Si₆ Particles in Al by Dynamic Electron Diffraction Studies, 277 (1997) 1221-1225.
[38] S.J. Andersen, C.D. Marioara, J. Friis, S. Wenner, R. Holmestad, Precipitates in aluminium alloys, Advances in Physics: X, 3 (2018) 1479984.